Acta Crystallographica Section F
**Structural Biology and Crystallization Communications**
ISSN 1744-3091

# Crystallization and preliminary X-ray diffraction of malate dehydrogenase from *Plasmodium falciparum*

**Carsten Wrenger,[a,b] Ingrid B. Müller,[b] Sabine Butzloff,[b] Rositsa Jordanova,[c] Sergey Lunev[c] and Matthew R. Groves[c]***

[a]Department of Parasitology, Institute of Biomedical Science, University of São Paulo, Avenida Professor Lineu Prestes 1374, 05508-000 Sao Paulo-SP, Brazil, [b]Biochemical Parasitology, Bernhard Nocht Institute for Tropical Medicine, Bernhard Nocht Strasse 74, D-20359 Hamburg, Germany, and [c]European Molecular Biology Laboratory – Hamburg Outstation c/o DESY, Building 25A, Notkestrasse 85, D-22670 Hamburg, Germany

Correspondence e-mail: groves@embl-hamburg.de

Received 20 February 2012
Accepted 3 April 2012

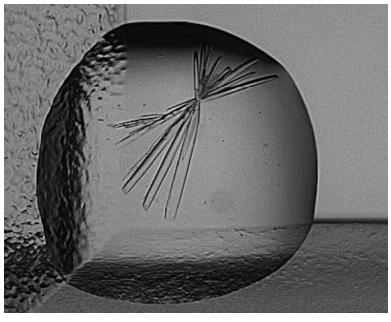



The expression, purification, crystallization and preliminary X-ray diffraction characterization of malate dehydrogenase (MDH) from the malarial parasite *Plasmodium falciparum* (*Pf*MDH) are reported. In order to gain a deeper understanding of the function and role of *Pf*MDH, the protein was purified to homogeneity. The purified protein crystallized in space group *P*1, with unit-cell parameters $a = 72$, $b = 157$, $c = 159$ Å, $\alpha = 105$, $\beta = 101$, $\gamma = 95^\circ$. The resulting crystals diffracted to a maximal resolution of 2.24 Å and the structure has been solved by molecular replacement, with 16 monomers in the asymmetric unit. The 16 monomers are arranged into four independent tetramers, in agreement with previous reports demonstrating the tetrameric solution state of *Pf*MDH. The X-ray structure of *Pf*MDH is expected to clarify the differences in catalysis by *Pf*MDH compared with other MDH family members and to provide a basis for the structure-based design of specific *Pf*MDH inhibitors as well as general MDH inhibitors.

## 1. Introduction

Malaria remains a pressing concern for global human health, and the lack of an effective vaccine as well as the spread of multi-drug-resistant strains requires the development of novel drug leads. Currently, the highly effective compound atovaquone, a constituent of the approved therapeutic Malerone, is known to interact with the $bc_1$ complex of the mitochondrial respiratory chain (Kessl *et al.*, 2003). Interestingly, recent publications have demonstrated the presence of a bifurcated tricarboxylic acid (TCA) cycle within the mitochondria of the parasite that is composed of both oxidative and reductive pathways (Olszewski & Llinás, 2011; Olszewski *et al.*, 2010). As a result, the malarial parasite does not cycle metabolites around a classical TCA pathway, but rather is dependent on the import and export of metabolites from the mitochondria in order to fuel carbon metabolism in the mitochondria.

The mitochondrial functions of the malaria parasite *Plasmodium falciparum* have recently attracted renewed interest, mainly because the genome sequence of the parasites revealed that genes encoding proteins that were thought to be irrelevant for parasite survival or development appear to be present in the parasite genome (Gardner *et al.*, 2002). In this context, the genes encoding the proteins that comprise the TCA cycle have been identified. However, the precise functions and localizations of some of the parasite proteins differ from those found in other eukaryotes. For instance, mitochondrial isocitrate dehydrogenase is an $NADP^+$-dependent enzyme that is most likely not to be a part of the parasite's TCA cycle but appears to play a role in redox regulation of the organelle (Wrenger & Müller, 2003). Furthermore, it has been shown that the pyruvate dehydrogenase, which is usually the link between cytosolic glycolysis and the mitochondrial TCA cycle, is located in the apicoplast of *P. falciparum*, where it provides acetyl-CoA and NADH for fatty-acid biosynthesis (Foth *et al.*, 2005). These data suggest that the roles of the enzymes predicted to be involved in certain metabolic pathways in the malaria parasites should be reassessed in order to define their precise functions in parasite metabolism.

Malate dehydrogenase (MDH) catalyses the reversible NAD(P)$^+$-dependent oxidation of oxaloacetate to malate. MDHs exist in multiple forms that differ in cofactor specificity and subcellular localization. Phylogenetic analyses of protozoan MDHs (EC 1.1.137) differentiated these enzymes into different classes, with a subdivision between mitochondrial and cytosolic MDHs (Roger *et al.*, 1999). MDHs are members of the NAD$^+$-dependent dehydrogenase family, which includes lactate dehydrogenases and alcohol dehydrogenases. These proteins are characterized by two functional domains, the catalytic domain and the NAD$^+$-binding domain, and are generally homodimeric or homotetrameric. However, mutants of MDHs also appear to be active in a monomeric form (Madern *et al.*, 2000). Madern and coworkers placed apicoplast MDHs at an evolutionary branch point between the MDH and lactate dehydrogenase (LDH) families by primary-sequence analysis and a comparison of the solution oligomeric state.

Despite the high degree of homology between the members of the NAD$^+$ dehydrogenase family, the enzymes are very specific for their respective substrates: MDHs have a high specificity for malate and oxaloacetate, whereas pyruvate and lactate are not accepted as substrates at an appreciable rate (Chapman *et al.*, 1999). Mitochondrial MDH is an integral part of the TCA cycle, providing oxaloacetate for the generation of citrate and NADH to fuel the mitochondrial electron-transport chain. However, *P. falciparum* does not possess a currently identified mitochondrial MDH, but rather a cytosolic MDH which supplies metabolites to the mitochondria and might be responsible for the generation of reducing equivalents, *e.g.* malate, to feed the respiratory chain (Wrenger *et al.*, 2012). The cytosolic enzyme serves in the provision of malate, which is transported into the mitochondrion *via* a potential malate/aspartate shuttle (Gardner, 2002). This shuttle system would allow the bidirectional transport of reducing equivalents between the cytosol and the mitochondrion and therefore overcomes the barrier of the inner mitochondrial membrane, which is impermeable to pyridine nucleotides.

In order to more fully understand the role of the cytosolic MDH of *P. falciparum* (*Pf*MDH), we have expressed, purified and crystallized *Pf*MDH and report the X-ray diffraction characterization of the crystals obtained.

## 2. Methods

### 2.1. Cloning of *Pf*MDH

The *MDH* gene of *P. falciparum* was amplified by polymerase chain reaction (PCR) using sequence-specific sense (5′-GCG CGC **GGTCTC** CAA TGA CTA AAA TTG CCT TAA TAG GTA GTG G-3′) and antisense (5′-GCG CGC **GGTCTC** AGC GCT TTA AAT GAT GAT GAT GAT GAT GAT GGC CTT TAA TTA AGT CGA AAG CTT TTT GTG-3′) oligonucleotides containing *Bsa*I restriction sites (indicated in bold) and *P. falciparum* 3D7 cDNA as template. The PCR was performed with *Pfu* polymerase using the following conditions: one cycle of 367 K for 7 min followed by 35 cycles of 1 min at 367 K, 1.5 min at 315 K and 2 min at 341 K. The PCR fragments were either cloned into TOPO Blunt (Invitrogen) or pASK-IBA3 previously digested with *Bsa*I and their nucleotide sequences were determined by automated sequencing (Seqlab, Germany). Nucleotide-sequence and protein-sequence analyses were performed using the *Gene Runner* software. The final construct consisted of full-length *Pf*MDH (PFF0895w; residues 1–313) with the additional amino acids GHHHHHHHLKR at the C-terminus.

### 2.2. Expression of *Pf*MDH

*Pf*MDH was recombinantly expressed in *Escherichia coli* BLR (DE3) (Novagen) using the expression plasmid pASK-IBA-MDH, which contains the open reading frame for the *MDH* gene fused to a C-terminal His tag to facilitate purification. Recombinant protein was purified *via* nickel-chelating chromatography employing the C-terminal His tag according to the manufacturer's recommendations. Transformed *E. coli* BLR (DE3) cells were propagated in selective medium (TB in the presence of 35 µg ml$^{-1}$ ampicillin) overnight at 310 K. The culture was induced at an $OD_{600}$ of 0.8 with 2 µg ml$^{-1}$ anhydrotetracycline. After induction, the temperature of the culture was lowered to 292 K and the cells were harvested by centrifugation (5500 rev min$^{-1}$ for 30 min) after overnight induction. All lysis, clarification and purification steps were performed at 277 K unless otherwise specified.

### 2.3. Purification of *Pf*MDH

The frozen cells from 3 l culture medium were suspended in 50 ml buffer *A* [50 m*M* bis-Tris pH 7.5, 250 m*M* NaCl, 20 m*M* imidazole, 10%(*v*/*v*) glycerol, 5 m*M* $\beta$-mercaptoethanol (BME)] supplemented with 10 units of DNAse. The cells were lysed by sonication and the homogenate was clarified by centrifugation at 19 000 rev min$^{-1}$ for 60 min.

The supernatant containing the soluble His-tagged protein was filtered using 0.22 µm Filtropur filters (Sarstedt) and incubated for 10 min with 15 ml Ni-charged affinity resin (Ni–NTA Agarose, Qiagen). The beads were poured into a gravity-flow column (Bio-Rad) and washed with 200 ml buffer *A*. The protein was eluted with 50 m*M* bis-Tris pH 7.5, 200 m*M* NaCl, 0.25 *M* imidazole, 10%(*v*/*v*) glycerol, 5 m*M* BME. The eluate was pooled and immediately dialyzed overnight at 277 K against 20 m*M* bis-Tris pH 6.5, 200 m*M* NaCl, 10%(*v*/*v*) glycerol, 5 m*M* BME.

The protein was concentrated to a volume of 2 ml and applied onto a HiLoad 16/60 Superdex 75 column (GE Healthcare) equilibrated with 50 m*M* bis-Tris pH 6.5, 150 m*M* NaCl, 5 m*M* BME. The gel-filtration buffer was chosen based upon a Thermofluor-based stability assay (Ericsson *et al.*, 2006; Nettleship *et al.*, 2008). The final purified protein eluted as a single peak with a retention time consistent with a tetrameric protein (data not shown). This peak was pooled and concentrated using a Spin-X UF concentration unit with a 10 kDa cutoff (Corning).

The final protein concentration was determined to be 10 mg ml$^{-1}$ based upon its theoretical absorbance at 280 nm [$Abs_{0.1\%}$(1 mg ml$^{-1}$) = 0.35; http://web.expasy.org/protparam/]. The final yield of purified *Pf*MDH was approximately 5 mg per litre of culture. The protein was concentrated and immediately used in crystallization trials. The protein purity was better than 95% as estimated using Coomassie Brilliant Blue-stained SDS–PAGE (Laemmli, 1970).

## 3. Results

### 3.1. Crystallization of *Pf*MDH

Concentrated protein was submitted to the EMBL Hamburg high-throughput crystallization facility (Mueller-Dieckmann, 2006) for initial screening against the Classics and Classics II Suites (Qiagen) sparse-matrix screening kits. Experiments were also performed in the presence of 1,8-ANS (Groves *et al.*, 2007; Watts *et al.*, 2010) to aid the identification of successful trials. All crystallization was performed at 293 K using equal volumes (200 nl) of protein solution

and crystallization reagent. Rod-shaped crystals of *Pf*MDH appeared one to two weeks after setting up crystallization experiments. Initial crystals were identified in 0.96 *M* sodium citrate pH 7.0 (Fig. 1*a*). Further optimization was performed at the same facility, using optimization screens designed around successful initial crystallization conditions in the absence of 1,8-ANS. The initial hit was optimized using an adapted solution-seeding method (D'Arcy *et al.*, 2007) in which the initial crystallization conditions were used as an additive (10%) for repeated sparse-matrix screening. After obtaining improved crystals in 0.096 *M* sodium citrate pH 7, 25%(*w*/*v*) PEG 3350, we obtained a final condition consisting of 0.1 *M* ammonium citrate pH 7, 22%(*w*/*v*) PEG 3350.

### 3.2. Diffraction data collection and processing

Optimized crystals were briefly transferred into a cryoprotective solution composed of 0.2 *M* ammonium citrate pH 7.0, 40%(*w*/*v*) PEG 3350. After a brief incubation period (5 s), the crystals were harvested from the cryoprotective solution into suitably sized cryoloops (Hampton Research). The mounted crystals were then flash-cooled in the nitrogen stream on beamline X13 at EMBL Hamburg (100 K) or plunge-cooled in liquid nitrogen prior to shipment to beamline BM14 at the ESRF. Initial frames (1 s exposure, 0 and 90° $\varphi$-axis rotation values) were used to characterize the crystals for optimal data-collection parameters using the software *BEST* (Bourenkov & Popov, 2006) as implemented in *DNA* (Incardona *et al.*, 2009). Data-collection parameters are indicated in Table 1.

Data were reduced using the *XDS* (Kabsch, 2010) and *SCALA* software (Evans, 2006). An analysis based on the Matthews coefficient (Matthews, 1968) predicted multiple copies of *Pf*MDH in the asymmetric unit. Accordingly, an $R_{\rm free}$ set (Brünger, 1992) for use in subsequent structure refinement and validation was created using 5% of the reflections populated from reflections in thin shells of equivalent resolution using the *DATAMAN* package (Kleywegt & Jones, 1996).

Molecular-replacement calculations were performed using the *MOLREP* package (Vagin & Teplyakov, 2010).

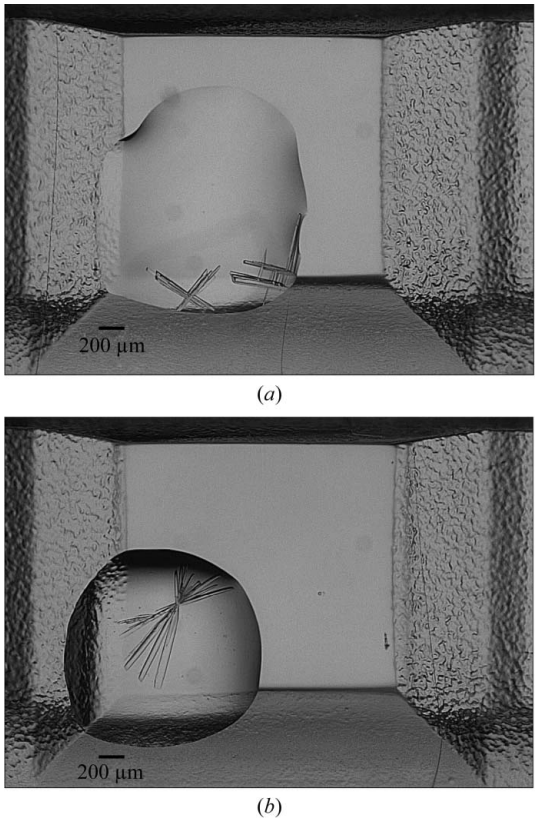


(*a*)

(*b*)

**Figure 1**
Images of (*a*) initial and (*b*) optimized crystals of *Pf*MDH grown at the EMBL high-throughput crystallization facility (Mueller-Dieckmann, 2006). Growth conditions are detailed in the text.

**Table 1**
Results of data collection from *Pf*MDH crystals.

Values in parentheses are for the highest resolution bin.

| | | |
|---|---|---|
| Data-collection parameters | | |
| Beamline | X13, EMBL Hamburg | BM14, ESRF |
| Wavelength (Å) | 0.8123 | 0.97841 |
| Temperature (K) | 100 | 100 |
| Oscillation range (°) | 0.25 | 0.3 |
| Crystal-to-detector distance (mm) | 266.27 | 253.45 |
| No. of frames | 999 | 650 |
| Exposure per frame (s) | 15 | 6 |
| Data-integration statistics | | |
| Space group | *P*1 | *P*1 |
| Unit-cell parameters (Å, °) | $a$ = 71.8, $b$ = 156.6, $c$ = 158.6, $\alpha$ = 104.6, $\beta$ = 101.0, $\gamma$ = 95.1 | $a$ = 72.4, $b$ = 155.3, $c$ = 159.1, $\alpha$ = 103.6, $\beta$ = 101.5, $\gamma$ = 95.2 |
| Resolution limits (Å) | 19.76–2.95 (3.12–2.95) | 47.62–2.24 (2.38–2.24) |
| Total No. of reflections | 326962 (35475) | 580251 (60206) |
| No. of unique reflections | 126210 (16058) | 273174 (31701) |
| Multiplicity | 2.59 (2.21) | 2.12 (1.90) |
| Completeness (%) | 92.0 (73.6) | 89.5 (64.3) |
| $R_{\rm merge}$† | 17.6 (64.8) | 5.3 (45.6) |
| Mean $I/\sigma(I)$ | 5.88 (1.42) | 10.46 (1.57) |
| $V_M$‡ (Å$^3$ Da$^{-1}$) | 3.08 | |
| Solvent content‡ (%) | 60.15 | |

† $R_{\rm merge}$ is defined as $\sum_{hkl}\sum_i |I_i(hkl) - \langle I(hkl)\rangle| / \sum_{hkl}\sum_i I_i(hkl)$, where $I_i(hkl)$ is the $i$th intensity measurement of reflection $hkl$ and $\langle I(hkl)\rangle$ is the average intensity from multiple observations. ‡ Based on 16 molecules per asymmetric unit.

## 4. Discussion

Rod-shaped crystals of *Pf*MDH appeared one to two weeks after setting up crystallization experiments using the EMBL Hamburg high-throughput crystallization facility (Mueller-Dieckmann, 2006). Initial crystals grown in 0.96 *M* sodium citrate pH 7.0 (Fig. 1*a*) diffracted to 2.77 Å resolution on beamline X13 at EMBL Hamburg (Table 1). The optimized crystals used for data collection (Fig. 1*b*, Table 1) had dimensions of 0.1 × 0.1 × 0.3 mm and diffracted to 2.24 Å resolution on beamline BM14 at the ESRF (Fig. 2, Table 1). Indexing algorithms determined that the *Pf*MDH crystals belonged to the primitive monoclinic system, with unit-cell parameters $a$ = 72.4, $b$ = 155.3, $c$ = 159.1 Å, $\alpha$ = 103.6, $\beta$ = 101.5, $\gamma$ = 95.2°.

The data-collection and reduction statistics for the *Pf*MDH crystal are reported in Table 1. Indicative diffraction patterns are shown in Fig. 2. Based on the molecular weight and the space group, it was inferred that there were 16 molecules of *Pf*MDH in the asymmetric unit of the crystal, which corresponds to a solvent content of about 56% (Matthews, 1968). Initial molecular-replacement trials using the data collected on beamline X13 at EMBL Hamburg were performed in *BALBES* (Long *et al.*, 2008) and a solution was found using the coordinates of MDH from *Cryptosporidium parvum* (PDB entry 2hjr; Vedadi *et al.*, 2007), which possesses 42.9% sequence identity over 309 residues, as a search model.

Molecular replacement using the data collected on beamline BM14 at the ESRF confirmed the correctness of the previously identified solution. The best solution for the higher resolution data (Tf/$\sigma$ score of 6.036, Tf contrast of 4.491), as well as acceptable $R$ and $R_{\rm free}$ values after the first refinement cycle (45.3 and 45.2, respectively), supported

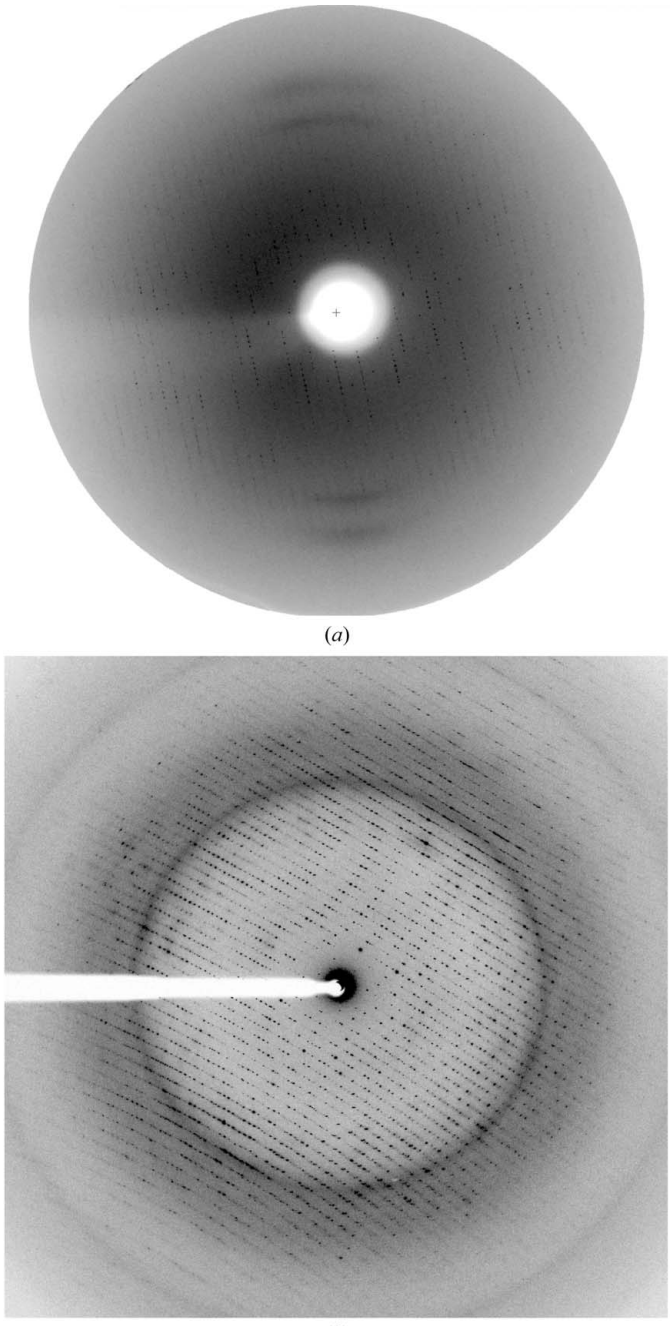

(*a*)

(*b*)

**Figure 2**
Examples of the diffraction obtained from the (*a*) unoptimized (beamline X13, EMBL Hamburg) and (*b*) optimized (beamline BM14, ESRF) crystals of *Pf*MDH. Data were collected from the unoptimized crystal and the optimized crystal harvested into a fibre loop and a Mylar loop, respectively. The maximum resolutions in (*a*) and (*b*) are 2.74 and 2.24 Å, respectively. The corresponding beamline parameters are indicated in Table 1.

the presence of four tetrameric *Pf*MDH assemblies in the asymmetric unit.

In this regard, it is pertinent to note that previous research on MDHs, for example those from *Flavobacterium frigidimaris* (Fujii *et al.*, 2007), *C. parvum* (Vedadi *et al.*, 2007) and a thermophilic *Bacillus* species (Wynne *et al.*, 1996), have shown that MDH displays a strong tendency to form oligomers and exists predominantly as tetramers, although isoforms of the enzyme from other species have been reported to be present as either dimers or tetramers in solution (Hunter *et al.*, 2000). Additionally, it has previously been reported that *Pf*MDH is a tetramer in solution (Pradhan *et al.*, 2009). Crystal structure refinement of *Pf*MDH is in progress and analysis of the structure will be reported elsewhere. The determined structure is likely to shed light on the differences in *Pf*MDH catalysis when compared with that of other MDH family members and to help in the structure-based design of specific *Pf*MDH inhibitors as well as general MDH inhibitors.

This work was supported by grants from the Deutsche Forschungsgemeinschaft (DFG; grant WR124/2) and the Fundação de Amparo à Pesquisa do Estado de São Paulo (FAPESP; grant 09/54325-2) to CW. X-ray data were collected on beamlines X13 at EMBL Hamburg and BM14 at the ESRF. We would like to thank Bärbel Bergmann for outstanding technical support and Drs J. Müller-Dieckmann and V. Lamzin for stimulating discussions. The authors would also like to thank the staff of beamline BM14 at the ESRF for their support during data collection.

## References

Bourenkov, G. P. & Popov, A. N. (2006). *Acta Cryst.* D**62**, 58–64.
Brünger, A. T. (1992). *Nature (London)*, **355**, 472–475.
Chapman, A. D., Cortés, A., Dafforn, T. R., Clarke, A. R. & Brady, R. L. (1999). *J. Mol. Biol.* **285**, 703–712.
D'Arcy, A., Villard, F. & Marsh, M. (2007). *Acta Cryst.* D**63**, 550–554.
Ericsson, U. B., Hallberg, B. M., DeTitta, G. T., Dekker, N. & Nordlund, P. (2006). *Anal. Biochem.* **357**, 289–298.
Evans, P. (2006). *Acta Cryst.* D**62**, 72–82.
Foth, B. J., Stimmler, L. M., Handman, E., Crabb, B. S., Hodder, A. N. & McFadden, G. I. (2005). *Mol. Microbiol.* **55**, 39–53.
Fujii, T., Oikawa, T., Muraoka, I., Soda, K. & Hata, Y. (2007). *Acta Cryst.* F**63**, 983–986.
Gardner, M. J. *et al.* (2002). *Nature (London)*, **419**, 498–511.
Groves, M. R., Müller, I. B., Kreplin, X. & Müller-Dieckmann, J. (2007). *Acta Cryst.* D**63**, 526–535.
Hunter, G. R., Hellman, U., Cazzulo, J. J. & Nowicki, C. (2000). *Mol. Biochem. Parasitol.* **105**, 203–214.
Incardona, M.-F., Bourenkov, G. P., Levik, K., Pieritz, R. A., Popov, A. N. & Svensson, O. (2009). *J. Synchrotron Rad.* **16**, 872–879.
Kabsch, W. (2010). *Acta Cryst.* D**66**, 125–132.
Kessl, J. J., Lange, B. B., Merbitz-Zahradnik, T., Zwicker, K., Hill, P., Meunier, B., Pálsdóttir, H., Hunte, C., Meshnick, S. & Trumpower, B. L. (2003). *J. Biol. Chem.* **278**, 31312–31318.
Kleywegt, G. J. & Jones, T. A. (1996). *Acta Cryst.* D**52**, 826–828.
Laemmli, U. K. (1970). *Nature (London)*, **227**, 680–685.
Long, F., Vagin, A. A., Young, P. & Murshudov, G. N. (2008). *Acta Cryst.* D**64**, 125–132.
Madern, D., Ebel, C., Mevarech, M., Richard, S. B., Pfister, C. & Zaccai, G. (2000). *Biochemistry*, **39**, 1001–1010.
Matthews, B. W. (1968). *J. Mol. Biol.* **33**, 491–497.
Mueller-Dieckmann, J. (2006). *Acta Cryst.* D**62**, 1446–1452.
Nettleship, J. E., Brown, J., Groves, M. R. & Geerlof, A. (2008). *Methods Mol. Biol.* **426**, 299–318.
Olszewski, K. L. & Llinás, M. (2011). *Mol. Biochem. Parasitol.* **175**, 95–103.
Olszewski, K. L., Mather, M. W., Morrisey, J. M., Garcia, B. A., Vaidya, A. B., Rabinowitz, J. D. & Llinás, M. (2010). *Nature (London)*, **466**, 774–778.
Pradhan, A., Mukherjee, P., Tripathi, A. K., Avery, M. A., Walker, L. A. & Tekwani, B. L. (2009). *Mol. Cell. Biochem.* **325**, 141–148.
Roger, A. J., Morrison, H. G. & Sogin, M. L. (1999). *J. Mol. Evol.* **48**, 750–755.
Vagin, A. & Teplyakov, A. (2010). *Acta Cryst.* D**66**, 22–25.
Vedadi, M. *et al.* (2007). *Mol. Biochem. Parasitol.* **151**, 100–110.
Watts, D., Müller-Dieckmann, J., Tsakanova, G., Lamzin, V. S. & Groves, M. R. (2010). *Acta Cryst.* D**66**, 901–908.
Wrenger, C., Müller, I. B., Silber, A. M., Jordanova, R., Lamzin, V. S. & Groves, M. R. (2012). *Curr. Drug Metab.* **13**, 332–336.
Wrenger, C. & Müller, S. (2003). *Eur. J. Biochem.* **270**, 1775–1783.
Wynne, S. A., Nicholls, D. J., Scawen, M. D. & Sundaram, T. K. (1996). *Biochem. J.* **317**, 235–245.